A Deep Learning Approach for Doppler Unfolding in Automotive TDM MIMO Radar

Ruxin Zheng, Hongshan Liu and Shunqiao Sun

Department of Electrical and Computer Engineering, The University of Alabama, Tuscaloosa, AL, USA
E-mails: {rzheng9,hliu75}@crimson.ua.edu, shunqiao.sun@ua.edu

2022 56th Asilomar Conference on Signals, Systems, and Computers | 978-1-6654-5906-8/22/$31.00 ©2022 IEEE | DOI: 10.1109/IEEECONF56349.2022.10051978

***Abstract*—Time-division multiplexing (TDM) is an easy way to achieve waveform orthogonality in automotive multiple-input multiple-output (MIMO) radar to synthesize a large virtual array to achieve high-resolution radar imaging for autonomous driving. Under TDM, only one transmit antenna is scheduled to transmit at each time slot. As a result, the maximum unambiguous detectable Doppler or radial speed is reduced by a factor of the number of transmit antennas. Additionally, there is phase migration in the array response for moving targets that needs to be compensated before angle estimation. The staggered pulse repetition intervals (PRIs) in consecutive frames can be used for Doppler unfolding. However, it has high computational complexity in pairing multiple targets. In this paper, we propose a fast and robust solution using a one-dimensional convolutional neural network to unfold the Doppler estimation in automotive TDM MIMO radar. The input of the neural network is the beam vector of the virtual array and the output is the unfolded velocity estimate for phase compensation. Extensive numerical experiments show that accurate Doppler estimation is achieved at a reasonable signal-to-noise ratio (SNR). Radar field experiments using Texas Instruments imaging radar support our theoretical investigations.**

***Index Terms*—automotive radar, MIMO radar, Doppler unfolding, deep learning, autonomous driving**

I. Introduction

The automotive radar sensor is a fundamental part of advanced driver assistance systems and autonomous vehicles largely because of its low cost, ability to sense during inclement weather, and immunity to poor visibility conditions [1]–[6]. Most automotive radar systems employ frequency-modulated continuous-wave (FMCW) transmit signals at the millimeter-wave band to achieve low-cost high-resolution sensing for complex functions during autonomous driving, such as automatic emergency braking, blind-spot detection, and adaptive cruise control [7], [8].

Multiple-input multiple-output (MIMO) radar technology is a cost-effective method and has been widely used to synthesize a large virtual array aperture for higher angular resolution using a small number of transmit and receive antennas [3], [9]–[11]. MIMO radar technology relies on the waveform orthogonality of the transmitted signals to enable separation at the receiving end. Waveform orthogonality can be achieved using various methods, such as time-division multiplexing (TDM), Doppler-division multiplexing (DDM), and frequency-division multiplexing (FDM) [3]. TDM is a simple way to achieve waveform orthogonality by scheduling one transmit antenna to transmit at each time slot. However, the maximum unambiguous detectable Doppler or equivalently the radial velocity is reduced by a factor of the number of transmit antennas. For imaging radar synthesized with a large number of transmit antennas, this problem becomes critical. Unfortunately, due to the reduction in maximum unambiguous detectable Doppler, moving targets with relatively high speeds are estimated with ambiguity. In addition, a phase migration is introduced for moving objects due to the switching delays among the transmit antennas from chirp to chirp, yielding distorted radar angular spectrum which would result in blurred radar imaging [3], [12].

This work was supported in part by U.S. National Science Foundation (NSF) under Grant CCF-2153386 and Alabama Transportation Institute (ATI).

Unlike cameras, which can overcome the blurred image issue by increasing frame per second, TDM MIMO radars require special antenna geometries or adaptive signal processing techniques to deal with phase migration. Phase error can be estimated using overlapping elements in the virtual aperture [13]. If two virtual elements corresponding to different transmitters share the same virtual position, the only phase difference between them in an ideal situation is that motion-induced phase error. However, this approach requires redundancy of virtual elements, which increases hardware cost. In addition, this approach suffers from low signal-to-noise ratio (SNR) situations. It was shown in [14] that overlapping elements are unnecessary and the motion compensation can be resolved via applying adaptive Discrete Fourier transform (DFT) on signals corresponding to different transmitters. However, such approach may cause ambiguities in the Doppler domain, and waveform design is required to achieve Doppler dealiasing. An approach with a staggered TDM configuration combined with Chinese remainder theorem (CRT) was proposed in [15] to unfold Doppler ambiguities. The transmitter is scheduled to transmit two consecutive frames with coprime pulse repetition intervals (PRIs), leading to different max unambiguous detectable velocities, respectively. With such different configurations, CRT is applied to identify the true Doppler estimation among all possible unfolded Doppler candidates under these two frames. This approach is robust, however, the paring process is computationally expensive.

In this paper, we propose a deep neural network approach to unfold the Doppler estimation in automotive TDM MIMO radar. Our innovations lie in the efficiency and robustness that are not enjoyed by traditional approaches that either need special staggered PRI or array configurations.

II. System Model of Automotive MIMO Radar

Frequency-modulated continuous-waveform (FMCW) is used in automotive radars, offering high-range resolution at low-cost that is unmatched by contemporary pulse-Doppler radars. In this section, we present FMCW radar principles and the system model of automotive MIMO radar to synthesize a large virtual array, followed by discussion of TDM MIMO radar challenges.

A. FMCW Radar

The transmit frequency of FMCW radar, $f_T(t)$, changes linearly with time, i.e.,

$$f_T(t) = f_c + \frac{B}{T}t, \tag{1}$$

where f_c, B, T are carry frequency, bandwidth and chirp duration, respectively. The phase $\varphi_T(t)$ of the transmitted signal could be

obtained after integration as $\varphi_T(t) = 2\pi \int_{-T/2}^{t} f_T(t)\,dt$. The noiseless received signal is a delayed version of transmit signal. For a target at a range of R with a radial velocity of v, the round-trip delay can be expressed as $\tau = 2(R + vt)/c$. The received signal is mixed with the transmit signal, and the output of the mixer is called *beat signal*, whose phase could be approximated as

$$\varphi_B(t) = 2\pi \left[\frac{2f_c R}{c} + \left(\frac{2f_c v}{c} + \frac{2BR}{Tc} \right) t \right], \tag{2}$$

where the beat frequency is $f_b = f_R + f_D$ with $f_R = \frac{2BR}{Tc}$ being the range frequency and $f_D = \frac{2f_c v}{c}$ being the Doppler frequency. The beat signal typically goes through a bandpass filter to compensate the gain for targets in distance to improve the radar dynamic range, followed by an analog-to-digital converter (ADC), whose sampling rate is greater than twice of maximum beat frequency $f_b^{\max}$. Range and Doppler information of the target could be obtained by applying fast Fourier transforms (FFTs) along fast-time and slow-time.

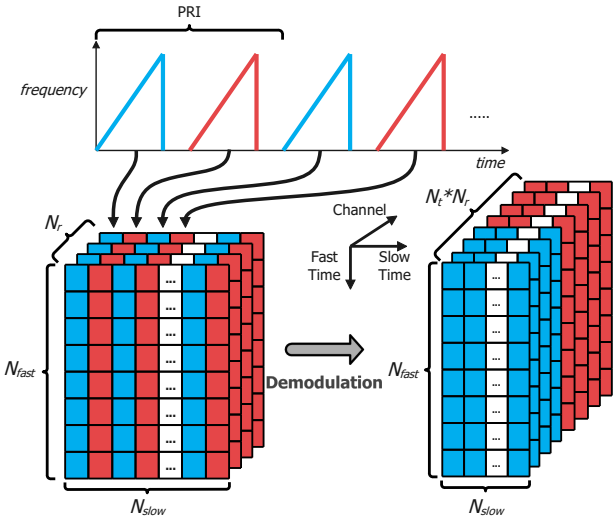

Fig. 1: Illustration of waveform orthogonality through TDM.

B. Automotive MIMO Radar and Waveform Orthogonality

MIMO radar can synthesize a large virtual array for angle estimation using a small number of transmit and multiple receive antennas [3], [9], thus has been adopted in automotive radar design [3]–[5]. Digital beamforming [16], or super-resolution algorithms, such as MUSIC [17], ESPRIT [18], compressive sensing [19], can be applied on the virtual array to estimate the DOA.

In automotive MIMO radar, it is desired to transmit orthogonal FMCW sequences so that at receiving side, the contribution of each transmit antenna can be extracted. There are different ways to achieve waveform orthogonality in MIMO radar, such as DDM and TDM [3]. In DDM, waveform orthogonality is achieved in the slow-time domain by multiplying a phase code on each transmitted FMCW chirp. At receive side, the contribution of each transmitter can be either shifted to higher Doppler frequency or treated as random noise by applying a slow-time Doppler demodulation after range FFT. DDM allows all transmit antennas to transmit simultaneously. However, it either reduces the maximum unambiguous detectable Doppler or masks objects with low radar cross-section by the waveform residual from other transmit antennas [3].

Under the TDM scheme, only one transmit antenna is selected to transmit at each time. A signal processing example of a TDM MIMO radar with $N_t = 2$ transmit antennas and $N_r = 4$ receive antennas is shown in Fig. 1. Assume there are N_{slow} chirps transmitted in one coherent processing interval (CPI) and the number of ADC samples is N_{fast}. All odd chirps (blue) are transmitted by the first transmit antenna; all even chirps (red) are transmitted by the second transmit antenna. At each receive antenna, the radar data matrix can be assembled into two matrices corresponding to odd and even chirp sequences, respectively. Therefore, a radar data cube with a dimension of $N_{\text{slow}}/N_t \times N_{\text{fast}} \times (N_t N_r)$ could be obtained from the original $N_{\text{slow}} \times N_{\text{fast}} \times N_r$ data cube. Due to its simplicity in implementation, in this paper, we adopt TDM to achieve waveform orthogonality.

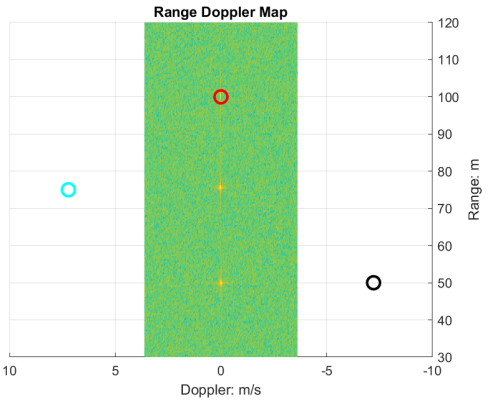

Fig. 2: Illustration of Doppler folding/aliasing. The FMCW radar simulator is configurated to have a maximum unambiguous detectable radial speed, $v_{\max} = 3.6$ m/s. Range-Doppler map with three targets at 100, 75, 50 meters with 0, $2v_{\max}$, $-2v_{\max}$. Circle markers show the targets' ground truth parameters.

C. Challenges of TDM MIMO Radar

1) Reduced Maximum Unambiguous Detectable Velocity: The maximum unambiguous detectable velocity of automotive radar is

$$v_{\max} = c/(4f_c T_{\text{PRI}}), \tag{3}$$

where c is the speed of light, while f_c and T_{PRI} denote the carrier frequency and PRI, respectively. In automotive TDM MIMO radar, since only one transmit antenna is scheduled to transmit pulse at each time slot, T_{PRI} of each transmit antenna is enlarged by the number of transmit antenna, N_t. As a result, $v_{\max}$ is reduced by N_t times.

2) Doppler Aliasing: For FMCW radar, when the targets move with velocity beyond $v_{\max}$, they appear on the range-Doppler map with aliasing. This phenomenon is also known as Doppler folding, since targets are folded back at incorrect locations within $[-v_{\max}, v_{\max}]$. We illustrate this problem in Fig 2. An FMCW radar simulator is used to generate radar data for three targets with different range and Doppler information. Although those three targets have different velocities, they share the same Doppler/velocity estimation on range-Doppler map due to Doppler folding. In this case, the velocity information of the object cannot be estimated accurately. For example, an object moving with aliasing velocity, such as $2v_{\max}$ or $-2v_{\max}$, could be detected as a stationary object.

3) Phase Migration: The scheduling delay, Δt, between different transmit antennas would cause phase migration for moving targets between different chirps, i.e.,

$$\phi = (4\pi/\lambda) v \Delta t. \tag{4}$$

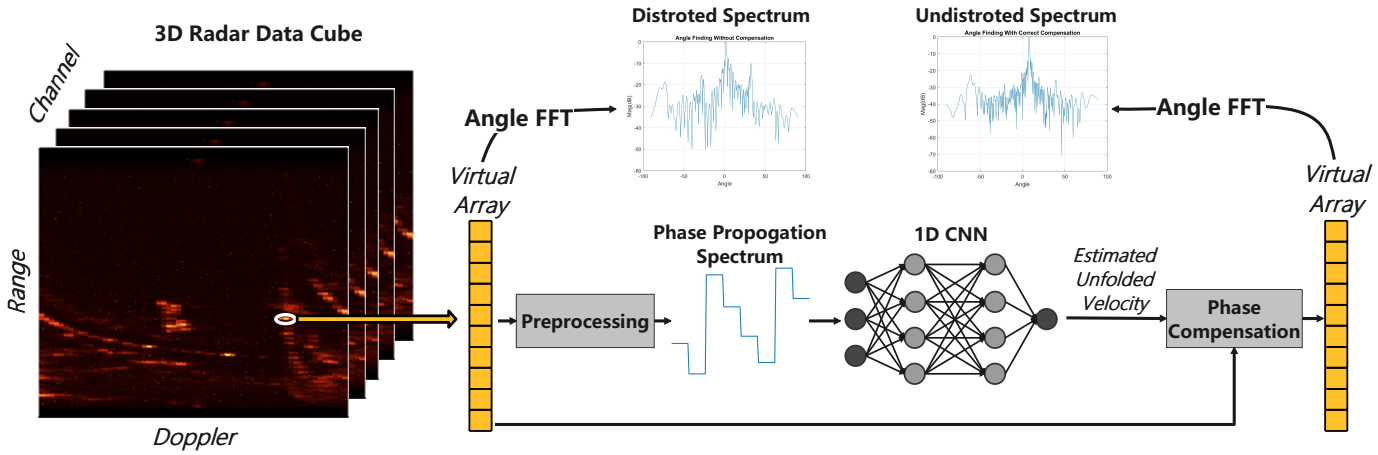

Fig. 3: The pipeline of Doppler unfolding using 1D CNN in automotive TDM MIMO radar.

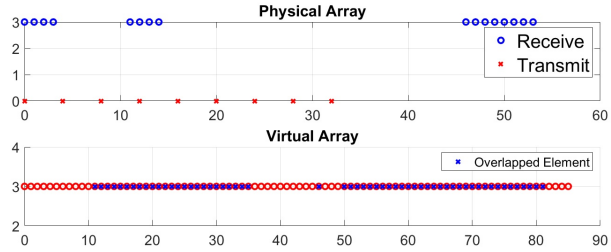

Fig. 4: The TI imaging radar. Four AWR2243 radar transceivers are cascaded together, providing 9 transmit and 16 receive antennas in the horizontal direction, enabling the synthesis of 86 unique virtual array elements with half-wavelength spacing. Note 58 virtual array elements are overlapped.

The phase migration creates a distortion in the virtual array beampattern, which may lead to inaccurate angle finding. We show this phenomenon via simulation with an array configuration, shown in Fig. 4, the same as Texas Instruments (TI) imaging radar [20]. Assume there is a moving target at 20° with $v = 10$ m/s. Fig. 5 (a) plots the angle spectrum obtained from the virtual array without velocity compensation. In order to remove phase migration, for every moving target, a compensation value $e^{-j\phi}$ needs to be multiplied along the virtual array before angle finding. Fig. 5 (b) shows the correct angle spectra after compensation.

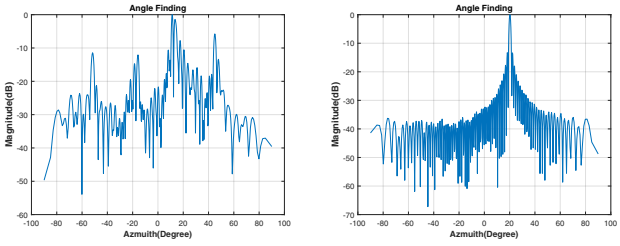

(a) (b)

Fig. 5: Angle spectra of a moving target with a velocity of 10 m/s and azimuth angle of 20°: (a) before and (b) after phase compensation. The radar is configured to select 9 transmit and 16 receive antennas with a chirp duration of 50 μs.

III. Doppler Unfolding Using Deep Neural Network

Theoretically, the velocity can be unfolded an infinite number of times. Fortunately, the typical velocity range in autonomous driving is within $[-120, 120]$ miles per hour. Therefore, when $v_{\max}$ is large enough, unfolding a limited number of times is sufficient. For example, the set of 9 possible unfolded velocities could be expressed as

$$\mathcal{S} = \{v - 4 \times (2v_{\max}), \cdots, v, \cdots, v + 4 \times (2v_{\max})\}. \quad (5)$$

The n-th element of the virtual uniform linear array with half-wavelength spacing corresponding to m-th transmit antenna can be expressed as

$$\mathbf{a}_n = e^{\left(\frac{2\pi(n-1)d}{\lambda}\sin\theta + (m-1)\phi\right)} + \text{noise}, \quad (6)$$

where ϕ is the phase migration defined in equation (4). Therefore, the phase difference along the virtual array is a feature that can be extracted for Doppler unfolding. We utilize a convolutional neural network (CNN) to unfold the Doppler estimation in automotive TDM MIMO radar. The neural network is first pre-trained with simulated data and then transfer-learning is carried out on real data. The same antenna configuration as the TI imaging radar is considered to generate the simulated data, which consists of beam vectors of virtual arrays obtained after range FFT followed by Doppler FFT. The dataset has 9 classes, where label 0 is the first velocity candidate and label 8 is the last velocity candidate.

The pipeline of Doppler unfolding using one-dimensional (1D) CNN in automotive TDM MIMO radar is shown in Fig. 3. First, the beam vector of the virtual array is selected from the three-dimensional radar data cube along the channel dimension. Next, in order to reduce the amount of data required for training, a signal preprocessing step that removes the angle-dependent phase in the virtual array beam vector is applied. The angle-dependent phase is derived from the phase difference using subarray, i.e., array elements corresponding to the same transmit antenna. Therefore, the input data for the Doppler unfolding network only contains motion-induced phase error, mutual coupling, and noise. Third, after the preprocessing step, phase features in the virtual array beam vector are extracted using a 1D CNN. The network consisting of three CNN layers and one fully connected layer, is proposed to classify virtual arrays such that the correct velocity can be estimated. The output of the network is the estimated velocity, which is then used to compensate for the

phase migration in the beam vector of the virtual array for accurate angle finding.

IV. Numerical Results and Radar Field Tests

A. Simulated Dataset & Real-World Dataset

To train and test the Doppler unfolding network, we create a simulated dataset and a real-world dataset. The simulated dataset is evenly distributed with 9 classes and contains $46,000$ beam vectors with different targets' radial speeds and directions of arrival using the same array geometry as TI cascade imaging radar. Moreover, field experiments are performed using TI imaging radar system on a 2021 Lexus RX450h vehicle platform shown in Fig. 6 (a). LiDAR and stereo cameras are used to provide velocity ground truth. For the real-world dataset, total $244,140$ beam vectors have been extracted from $1,700$ frames of the 3D radar data cube. The SNR of the beam vector is estimated as $\text{SNR} = 10\log_{10}(\mathbf{S}^2/\mathbf{N}^2)$, where $\mathbf{S}$ denotes signal amplitude and $\mathbf{N}$ denotes noise floor from range-Doppler spectrum of each channel. Range-Doppler two-dimensional FFTs yield a signal processing gain [3] of $10\log_{10}(N_{\text{fast}}N_{\text{slow}}) = 42.14$ dB, where $N_{\text{fast}} = 256$ and $N_{\text{slow}} = 64$ are the number of samples in fast-time and slow-time, respectively. The dataset class distribution and SNR distribution are shown in Fig. 6 (c) and (d).

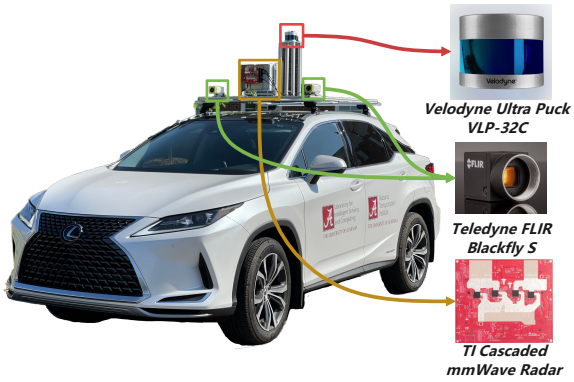

(a)

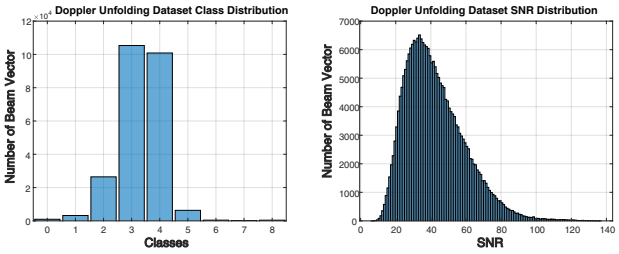

(b) (c)

Fig. 6: (a) Multi-modal sensor configuration on a 2021 Lexus RX450h vehicle platform for field experiments.; (b) Real-World Dataset class distribution.; (c) Real-World Dataset SNR distribution.

B. Doppler Unfolding Network Performance Evaluation

The Doppler unfolding network is first trained with the simulated dataset. The performance is evaluated using multiple simulated test sets with different noise levels. The confusion matrix of three simulated test sets with 10dB and 15dB respectively is shown in Fig.7.

To increase the network performance on real-world data, we take a small training set that contains 900 samples with evenly distributed

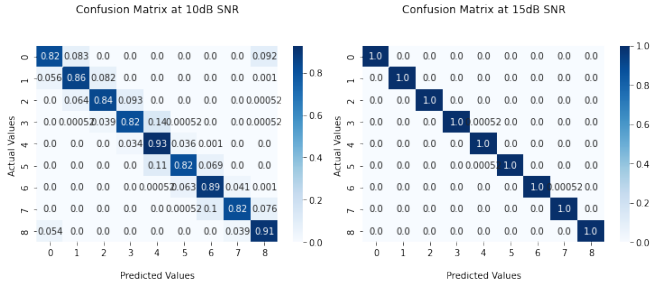

(a) (b)

Fig. 7: Confusion matrix under different SNR configurations.

classes from the real-world dataset to train the pre-trained network. The proposed model predicts with 93.46% accuracy. The confusion matrix of the real-world dataset is shown in Fig. 8.

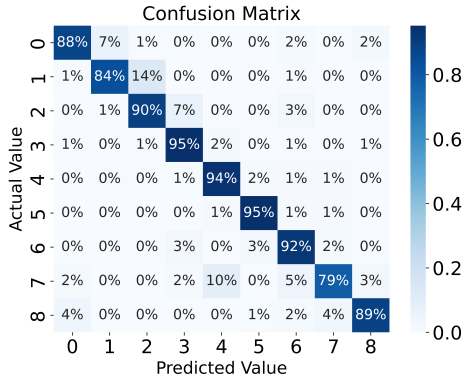

Fig. 8: Confusion Matrix of Real-World Dataset.

C. Examples of Radar Imaging With and Without Compensation

Radar bird's-eye-view (BEV) examples with and without compensation under various driving scenarios are shown in Fig. 9. Here, the radar BEV is first obtained as range-azimuth spectra in Polar coordinate and then transformed into Cartesian coordinate. It is shown that when driving at high speeds on a highway, radar BEVs are severely affected by motion-induced phase errors. The blur effect is significantly suppressed after compensation with the correct velocity predicted by the proposed Doppler unfolding network. For example, after compensation, the false targets due to the high sidelobes introduced by the motion are successfully mitigated. We also include some intersection examples, where most targets are stationary or with low velocities and thus no compensation is required. In summary, the "motion-blur" effect of automotive TDM MIMO radar imaging can be successfully suppressed under the proposed deep learning-aided signal processing chain for various driving scenarios.

V. Conclusion

In this work, we developed a deep learning approach for solving the Doppler unfolding issue in automotive TDM MIMO radar. A simulated and a real-world dataset were created for training and testing the Doppler unfolding network. We have shown that our Doppler unfolding network achieves 93.46% accuracy on the real-world dataset, and is able to robustly generate undistorted radar BEVs containing rich object features under various driving scenarios.

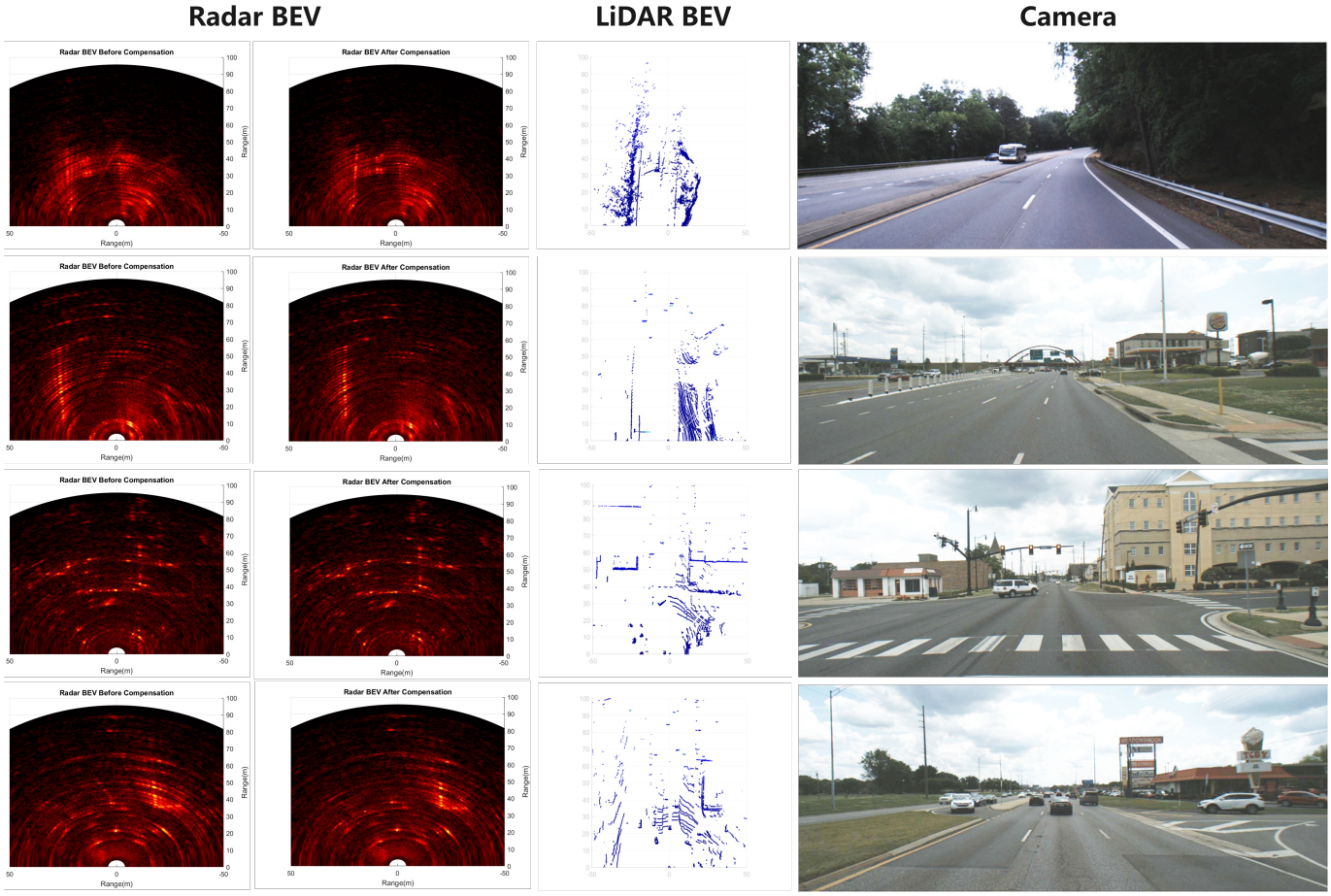

Fig. 9: Radar imaging examples. Radar BEVs are shown in the first column (before velocity compensation) and the second column (after velocity compensation via Doppler unfolding network). LiDAR point clouds are shown in BEV format in the third column. Due to limited space, only the image from the left camera is shown in the fourth column.

REFERENCES

[1] S. Patole, M. Torlak, D. Wang, and M. Ali, "Automotive radars: A review of signal processing techniques," *IEEE Signal Processing Magazine*, vol. 34, no. 2, pp. 22–35, 2017.

[2] F. Engels, P. Heidenreich, A. M. Zoubir, F. K. Jondral, and M. Wintermantel, "Advances in automotive radar: A framework on computationally efficient high-resolution frequency estimation," *IEEE Signal Processing Magazine*, vol. 34, no. 2, pp. 36–46, 2017.

[3] S. Sun, A. P. Petropulu, and H. V. Poor, "MIMO radar for advanced driver-assistance systems and autonomous driving: Advantages and challenges," *IEEE Signal Processing Magazine*, vol. 37, no. 4, pp. 98–117, 2020.

[4] C. Waldschmidt, J. Hasch, and W. Menzel, "Automotive radar — From first efforts to future systems," *IEEE Journal of Microwaves*, vol. 1, no. 1, pp. 135–148, 2021.

[5] M. Markel, *Radar for Fully Autonomous Driving*. Boston, MA: Artech House, 2022.

[6] Z. Peng, C. Li, and F. Uysal, *Modern Radar for Automotive Applications*. London, UK: IET, 2022.

[7] S. Sun and Y. D. Zhang, "4D automotive radar sensing for autonomous vehicles: A sparsity-oriented approach," *IEEE Journal of Selected Topics in Signal Processing*, vol. 15, no. 4, pp. 879–891, 2021.

[8] G. Duggal, S. Vishwakarma, K. V. Mishra, and S. S. Ram, "Doppler-resilient 802.11ad-based ultrashort range automotive joint radar-communications system," *IEEE Transactions on Aerospace and Electronic Systems*, vol. 56, no. 5, pp. 4035–4048, 2020.

[9] J. Li and P. Stoica, "MIMO radar with colocated antennas," *IEEE Signal Process. Mag.*, vol. 24, no. 5, pp. 106–114, 2007.

[10] ——, *MIMO Radar Signal Processing*. Hoboken, NJ, Wiley, 2009.

[11] J. Bergin and J. R. Guerci, *MIMO Radar: Theory and Application*. Boston, MA, Artech House, 2018.

[12] S. L. Cassidy, S. Pooni, M. Cherniakov, E. G. Hoare, and M. S. Gashinova, "High resolution automotive imaging using MIMO radar and Doppler beam sharpening," *IEEE Transactions on Aerospace and Electronic Systems*, to appear, 2022.

[13] C. M. Schmid, R. Feger, C. Pfeffer, and A. Stelzer, "Motion compensation and efficient array design for TDMA FMCW MIMO radar systems," in *2012 6th European Conference on Antennas and Propagation (EUCAP)*. IEEE, 2012, pp. 1746–1750.

[14] J. Bechter, F. Roos, and C. Waldschmidt, "Compensation of motion-induced phase errors in TDM MIMO radars," *IEEE Microwave and Wireless Components Letters*, vol. 27, no. 12, pp. 1164–1166, 2017.

[15] R. Zheng, S. Sun, D. Scharff, and T. Wu, "Spectranet: A high resolution imaging radar deep neural network for autonomous vehicles," in *IEEE Sensor Array and Multichannel Signal Processing Workshop (SAM)*, Trondheim, Norway, June 20-23, 2022, pp. 301–305.

[16] S. Tokoro, K. Kuroda, A. Kawakubo, K. Fujita, and H. Fujinami, "Electronically scanned millimiter-wave radar for precrash safety and adaptive cruise control system," in *Proc. IEEE Intelligent Vehicles Symposium*, Columbus, OH, June 2003.

[17] R. Schmidt, "Multiple emitter location and signal parameter estimation," *IEEE Trans. Antennas Propag.*, vol. 34, no. 3, pp. 276–280, 1986.

[18] R. Roy and T. Kailath, "ESPRIT - estimation of signal parameters via rotation invariance techniques," *IEEE Trans. Acoust., Speech, Signal Process.*, vol. 17, no. 7, pp. 984–995, 1989.

[19] E. J. Candès and T. Tao, "The Dantzig selector: Statistical estimation when p is much larger than n," *The Annals of Statistics*, vol. 35, no. 6, pp. 2313–2351, 2007.

[20] Texas Instruments, *Design Guide: TIDEP-01012 Imaging Radar Using Cascaded MmWave Sensor Reference Design*, 2020, rev. A. [Online]. Available: https://www.ti.com/lit/ug/tiduen5a/tiduen5a.pdf